



# Influences of light and humidity on carbonyl sulfide-based estimates of photosynthesis

Linda M. J. Kooijmans<sup>a,1,2</sup>, Wu Sun<sup>b</sup>, Juho Aalto<sup>c,d</sup>, Kukka-Maaria Erkkilä<sup>c</sup>, Kadmiel Maseyk<sup>e</sup>, Ulrike Seibt<sup>b</sup>, Timo Vesala<sup>c,f</sup>, Ivan Mammarella<sup>c</sup>, and Huilin Chen<sup>a,2</sup>

<sup>a</sup>Centre for Isotope Research, University of Groningen, 9747 AG, Groningen, The Netherlands; <sup>b</sup>Department of Atmospheric and Oceanic Sciences, University of California, Los Angeles, CA 90095-1565; <sup>c</sup>Faculty of Science, Institute for Atmospheric and Earth System Research/Physics, University of Helsinki, 00014 Helsinki, Finland; <sup>d</sup>Station for Measuring Forest Ecosystem–Atmosphere Relations II, Hyytiälä Forestry Field Station, University of Helsinki, 35500 Korkeakoski, Finland; <sup>e</sup>School of Environment, Earth and Ecosystem Sciences, The Open University, MK 7 6AA Milton Keynes, United Kingdom; and <sup>f</sup>Faculty of Agriculture and Forestry, Institute for Atmospheric and Earth System Research/Forest Sciences, University of Helsinki, 00014 Helsinki, Finland

Edited by Steven C. Wofsy, Harvard University, Cambridge, MA, and approved December 18, 2018 (received for review May 2, 2018)

**Understanding climate controls on gross primary productivity (GPP) is crucial for accurate projections of the future land carbon cycle. Major uncertainties exist due to the challenge in separating GPP and respiration from observations of the carbon dioxide (CO<sub>2</sub>) flux. Carbonyl sulfide (COS) has a dominant vegetative sink, and plant COS uptake is used to infer GPP through the leaf relative uptake (LRU) ratio of COS to CO<sub>2</sub> fluxes. However, little is known about variations of LRU under changing environmental conditions and in different phenological stages. We present COS and CO<sub>2</sub> fluxes and LRU of Scots pine branches measured in a boreal forest in Finland during the spring recovery and summer. We find that the diurnal dynamics of COS uptake is mainly controlled by stomatal conductance, but the leaf internal conductance could significantly limit the COS uptake during the daytime and early in the season. LRU varies with light due to the differential light responses of COS and CO<sub>2</sub> uptake, and with vapor pressure deficit (VPD) in the peak growing season, indicating a humidity-induced stomatal control. Our COS-based GPP estimates show that it is essential to incorporate the variability of LRU with environmental variables for accurate estimation of GPP on ecosystem, regional, and global scales.**

carbonyl sulfide | photosynthesis | stomatal conductance | carbon cycle

Carbonyl sulfide (COS) follows the same diffusion pathway into the leaf chloroplasts as CO<sub>2</sub> and is consumed by the enzyme carbonic anhydrase (CA) (1, 2). The hydrolysis of COS via CA is irreversible (3), such that no respiration-like COS flux is evident under ambient conditions. Consequently, the atmospheric drawdown of COS above an ecosystem reflects the uptake of COS by plants, provided that other sources and sinks in the ecosystem are negligible or known. The dominant vegetative sink of COS was therefore recognized as a way to separate net ecosystem exchange of CO<sub>2</sub> (NEE) into gross primary productivity (GPP) and respiration (4–7). With a known ratio of COS to CO<sub>2</sub> uptake at the leaf level, GPP can be determined from COS ecosystem fluxes (F<sub>COS-E</sub>) following (5, 7):

$$GPP_{COS} = -F_{COS-E} \frac{C_{a,CO_2}}{C_{a,COS}} \frac{1}{LRU}, \quad [1]$$

with atmospheric mole fractions C<sub>a,COS</sub> and C<sub>a,CO<sub>2</sub></sub>, and the leaf-scale relative uptake ratio (LRU) = F<sub>COS</sub>/F<sub>CO<sub>2</sub></sub> · C<sub>a,CO<sub>2</sub></sub>/C<sub>a,COS</sub> at the leaf level). LRU is also referred to as the ratio of deposition velocities of COS and CO<sub>2</sub> (8). The accuracy of LRU is key in translating COS fluxes into GPP, and several studies have derived LRU for different plant species from chamber enclosure measurements (8–17). Those LRU values ranged from 0.4 to 9.5 with a median of 1.75 and with 50% of the values between 1.48 and 2.46 around the median (see ref. 18 for an overview).

Many of the laboratory studies measured LRU under constant conditions and few have investigated LRU response to environmental variations or under field conditions (13, 17). If effects of light, humidity, and temperature on dissolution, diffusion, and relevant enzyme reactions differ between COS and CO<sub>2</sub>, then LRU should be expected to vary (13). It has already been found that LRU changes with light intensity (13, 14, 17, 19, 20). This is due to the light independence of the CA enzyme that controls F<sub>COS</sub> (14, 21, 22), whereas F<sub>CO<sub>2</sub></sub> depends on the light reactions in the photosystems.

LRU values are typically larger than 1.0, which implies that the deposition velocities of COS are typically higher than those of CO<sub>2</sub>. This is attributed to a lower reaction efficiency of ribulose-1,5-bisphosphate carboxylase/oxygenase with CO<sub>2</sub> than that of CA with COS (9, 12), which can be expected because CA is known to be the enzyme with the highest molar activity (2).

## Significance

Carbonyl sulfide (COS) measurements enable quantification of terrestrial photosynthesis, which cannot be directly measured at scales greater than the leaf level. The accuracy of COS-based estimates of gross primary production (GPP) depends on how we relate the COS uptake to that of CO<sub>2</sub>. This study shows that COS-based GPP estimates will be significantly overestimated if the different environmental responses of COS and CO<sub>2</sub> uptake are not taken into account. These findings are relevant for studies that rely on COS to quantify ecosystem to regional scale GPP, and support the use of a COS-based approach to constrain ecosystem flux partitioning. Moreover, the strong stomatal control on COS uptake shown in this study makes COS a suitable tracer for stomatal diffusion.

Author contributions: L.M.J.K., W.S., J.A., K.-M.E., K.M., U.S., T.V., I.M., and H.C. designed research; L.M.J.K., W.S., J.A., K.-M.E., K.M., and H.C. performed research; L.M.J.K., W.S., J.A., K.-M.E., and H.C. analyzed data; and L.M.J.K., W.S., J.A., K.-M.E., K.M., U.S., T.V., I.M., and H.C. wrote the paper.

The authors declare no conflict of interest.

This article is a PNAS Direct Submission.

This open access article is distributed under Creative Commons Attribution-NonCommercial-NoDerivatives License 4.0 (CC BY-NC-ND).

Data deposition: The data used in this work are available from <https://zenodo.org/record/1211481#.XB4Lb9IzBIU>. The dataset includes branch fluxes and mole fractions of COS and CO<sub>2</sub>, LRU, stomatal conductance, internal conductance, eddy-covariance fluxes of COS and CO<sub>2</sub>, GPP, and meteorological information. The code used to calculate the chamber fluxes from measured mole fractions is available from <https://zenodo.org/record/1197330#.XB4OLNlzbIU>. The code used to generate the main results in this work is available from <https://zenodo.org/record/1211499#.XB4PStIzBIU>.

<sup>1</sup>Present address: Meteorology and Air Quality Group, Wageningen University and Research Centre 6700 AA, Wageningen, The Netherlands.

<sup>2</sup>To whom correspondence may be addressed. Email: linda.kooijmans@wur.nl or huilin.chen@rug.nl.

This article contains supporting information online at [www.pnas.org/lookup/suppl/doi:10.1073/pnas.1807600116/-DCSupplemental](http://www.pnas.org/lookup/suppl/doi:10.1073/pnas.1807600116/-DCSupplemental).

Published online January 25, 2019.

Therefore, COS uptake is not expected to be strongly limited by biochemical reactions, unlike  $\text{CO}_2$  uptake, which is limited by light reactions in the photosystems. As a result, the stomatal conductance should be a more limiting component for  $F_{\text{COS}}$  than for  $F_{\text{CO}_2}$ , which makes LRU dependent on stomatal conductance (17). In line with this hypothesis, it has been found that a further decrease of LRU at high radiation levels may occur under conditions of increasing vapor pressure deficit (VPD) and lower stomatal conductance in the afternoon (17). Furthermore, the fact that COS and  $\text{CO}_2$  do not share the photochemical reaction in the leaf, but only the diffusive pathway between air and the chloroplast, has recently motivated the use of COS as a tracer for diffusive conductance, of which the stomatal conductance is the dominant component (20, 23).

In this study, we aim to characterize  $F_{\text{COS}}$  at the branch level under field conditions and investigate if  $F_{\text{COS}}$  and  $F_{\text{CO}_2}$  respond similarly to environmental changes. We performed continuous COS and  $\text{CO}_2$  branch chamber measurements over 5 mo during spring recovery and early summer in 2017 in a boreal forest in Finland, making this a study investigating  $F_{\text{COS}}$  at the branch level over different phenological stages. This dataset allows us to test the applicability of findings from previous studies—which were confined to laboratory conditions or field measurements over a short period of time—to different phenological stages and environmental conditions. With the different components of  $F_{\text{COS}}$  (ecosystem, soil, and branch fluxes) being characterized at the site, we are able to derive COS-based GPP estimates and test the effect of the variability of LRU on GPP.

## Results and Discussion

**Responses of  $F_{\text{COS}}$  and  $F_{\text{CO}_2}$  to Light and Stomatal Conductance.** Both  $F_{\text{COS}}$  and  $F_{\text{CO}_2}$  show a strong diurnal cycle with a sink during the daytime (Fig. 1A). The increase of COS uptake (more negative  $F_{\text{COS}}$ ) early in the morning coincides with the increase of stomatal conductance ( $g_{s,\text{COS}}$ ), whereas the increase of  $F_{\text{CO}_2}$  lags behind due to its light dependence. The peak of  $F_{\text{COS}}$  is typically 1 h earlier than that of  $F_{\text{CO}_2}$  (Fig. 1A), which was also observed by Geng and Mu (24) in a Chinese deciduous forest. Unlike  $F_{\text{CO}_2}$ ,  $F_{\text{COS}}$  shows continued uptake during nighttime of  $-1.44 \pm 0.95 \text{ pmol m}^{-2}\text{s}^{-1}$  (median  $\pm$  SD) in May–July (Fig. 1A). The different responses of  $F_{\text{COS}}$  and  $F_{\text{CO}_2}$  to light is also evident from Fig. 2A and B;  $F_{\text{CO}_2}$  increases with the photosynthetically active radiation (PAR) up to  $\sim 700 \text{ } \mu\text{mol m}^{-2}\text{s}^{-1}$ , whereas  $F_{\text{COS}}$  increases up to a PAR value of  $\sim 200 \text{ } \mu\text{mol m}^{-2}\text{s}^{-1}$ . The light dependence of  $F_{\text{CO}_2}$  is caused by two distinct processes: (i) carbon fixation depends on the light reactions in the photosystems (25) and (ii) stomatal aperture, which controls the intercellular  $\text{CO}_2$  available for fixation, increases with light as a strategy to optimize carbon gain against water loss (26, 27). In contrast to  $\text{CO}_2$ , the COS biochemical reactions are light independent (14, 21, 22), but  $F_{\text{COS}}$  responds to light solely due to the light response of stomatal conductance.

$F_{\text{COS}}$  and  $F_{\text{CO}_2}$  peak early in the morning when VPD is still low and  $g_{s,\text{COS}}$  is high (Fig. 1A and C), which confirms a shared stomatal control on both fluxes. We find strong correlations of  $F_{\text{COS}}$  with  $g_{s,\text{COS}}$  at all light levels and even during night (Fig. 2E and F). This is strong evidence that  $F_{\text{COS}}$  could provide a means to constrain stomatal conductance—during both day and night—and therefore links to both the carbon and water cycles (23). However, we also find that, at high light levels, the increase of  $F_{\text{COS}}$  with  $g_{s,\text{COS}}$  is smaller than at low light levels (Fig. 2E and F). This suggests that during the daytime  $F_{\text{COS}}$  is colimited by nonstomatal resistances, which will be further discussed in the next section.

In the correlation with PAR, we find a decrease of COS uptake (less negative  $F_{\text{COS}}$ ) toward higher light levels (Fig. 2A and B) that is consistent with a decrease of  $g_{s,\text{COS}}$  (SI Appendix, Fig. S2), while on average  $F_{\text{CO}_2}$  remains constant. This is in line with the hypothesis that the stomatal closure would affect  $F_{\text{COS}}$  more than it would affect  $F_{\text{CO}_2}$  because the stomatal conductance is a more dominant component for  $F_{\text{COS}}$  than it is for  $F_{\text{CO}_2}$  (17). This

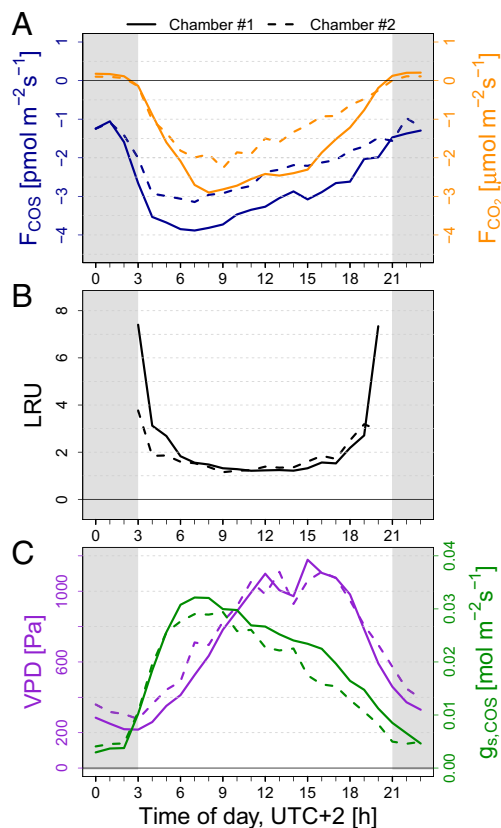


**Fig. 1.** Average diurnal cycles of  $F_{\text{COS}}$  and  $F_{\text{CO}_2}$  (A), LRU (B), and  $g_{s,\text{COS}}$  and VPD (C) between 18 May and 13 July 2017 (the peak season), for chambers 1 (solid) and 2 (dashed).  $g_{s,\text{COS}}$  is determined in two ways: daytime  $g_{s,\text{COS}}$  (solar elevation angle  $> 0^\circ$ ) is determined from the Ball–Berry model, nighttime  $g_{s,\text{COS}}$  (solar elevation angle  $< 0^\circ$ , shaded) is determined from transpiration measurements (Methods)—both independent of  $F_{\text{COS}}$ . We report stomatal conductance as that to COS ( $g_{s,\text{COS}}$ ), which relates to stomatal conductance to  $\text{H}_2\text{O}$  ( $g_{s,\text{H}_2\text{O}}$ ) through  $g_{s,\text{COS}} = g_{s,\text{H}_2\text{O}}/2.00$ , where the value 2.00 is the ratio of  $\text{H}_2\text{O}$  and COS diffusivities (12). Time series of  $F_{\text{COS}}$ ,  $F_{\text{CO}_2}$ , LRU, and meteorological parameters can be found in SI Appendix, Fig. S1.

may also explain why the peak of  $F_{\text{COS}}$  occurs earlier than that of  $F_{\text{CO}_2}$  (Fig. 1A);  $F_{\text{COS}}$  becomes more limited as VPD increases and  $g_{s,\text{COS}}$  is limited (Fig. 1C), whereas  $F_{\text{CO}_2}$  can continue to increase due to increasing PAR.

LRU varies largely over a day, which reflects the fact that COS uptake is light independent, whereas  $\text{CO}_2$  uptake is restricted under low light conditions, e.g., around sunrise and sunset (Fig. 1B). Therefore, LRU decreases exponentially toward high PAR (Fig. 2C and D), which is similar to the findings in Stimler et al. (14) and Sun et al. (17). The variation of LRU with PAR largely explains the variation of daytime LRU between days (SI Appendix, Fig. S1). Moreover, LRU does not become constant toward high light conditions (Fig. 2C and D, Insets), which was also observed by Sun et al. (17) for vegetation in a freshwater marsh. At high light levels we find a correlation between LRU and VPD ( $P < 0.01$ ) and between LRU and  $g_{s,\text{COS}}$  ( $P < 0.05$ ) in the peak of the growing season (SI Appendix, Fig. S3), which is likely due to the different responses of  $F_{\text{COS}}$  and  $F_{\text{CO}_2}$  to  $g_{s,\text{COS}}$ . These findings support that differential stomatal limitations on  $F_{\text{COS}}$  and  $F_{\text{CO}_2}$  drive LRU variation.

The light-saturated LRU (for  $\text{PAR} > 700 \text{ } \mu\text{mol m}^{-2}\text{s}^{-1}$ ) is on average 1.1, which is on the lower end of LRU values reported in previous studies (see ref. 18 for an overview). Note that previous LRU measurements could have been affected by the dependence of LRU to PAR. LRU values have not always been determined at high light levels, which would have led to overestimated LRU. For

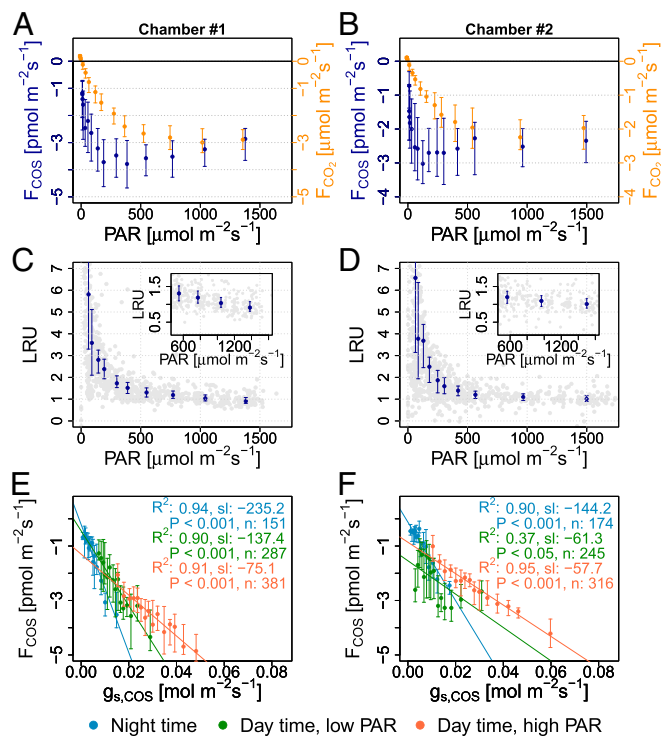


**Fig. 2.** Responses of  $F_{\text{CO}_2}$ ,  $F_{\text{CO}_2}$ , and LRU to light and of  $F_{\text{CO}_2}$  to  $g_{\text{s,COS}}$ . Average  $F_{\text{CO}_2}$ ,  $F_{\text{CO}_2}$  (A and B) and LRU (C and D) versus PAR, and  $F_{\text{CO}_2}$  versus  $g_{\text{s,COS}}$  (E and F) from 18 May to 13 July for chambers 1 (Left) and 2 (Right). Data are plotted as the median of 15 equal-sized bins in the x range. The error bars represent the 25th and 75th percentiles of data in each bin. For the correlation of  $F_{\text{CO}_2}$  with  $g_{\text{s,COS}}$  (E and F) the different colors represent different light conditions: nighttime (blue); daytime with low light conditions (PAR < 150 and 100  $\mu\text{mol m}^{-2}\text{s}^{-1}$  for chambers 1 and 2, respectively; green); daytime with high light conditions (PAR > 300  $\mu\text{mol m}^{-2}\text{s}^{-1}$ ; orange). A transition phase between low and high PAR values is neglected. The coefficient of determination ( $R^2$ ), slope (sl), significance level (P), and number of data (n) are given for a linear regression through the median values (E and F).

example, Kesselmeier and Merk (9) determined LRU at a light level of 300  $\mu\text{mol m}^{-2}\text{s}^{-1}$  and Sandoval-Soto et al. (8) also measured LRU in Scots pine but at a light level of 600  $\mu\text{mol m}^{-2}\text{s}^{-1}$  where  $F_{\text{CO}_2}$  is not PAR saturated.

**Internal Conductance of COS Limits  $F_{\text{CO}_2}$  During Daytime.** We estimated the internal conductance to COS ( $g_{\text{i,COS}}$ ), which is a combination of nonstomatal conductance terms, and find that during daytime  $g_{\text{i,COS}}$  is smaller than  $g_{\text{s,COS}}$  (see *SI Appendix, Fig. S4* and the accompanying explanation). The ratio of  $g_{\text{s,COS}}$  over  $g_{\text{i,COS}}$  determines the relative importance of the two conductances on  $F_{\text{CO}_2}$  and thereby also on LRU (see equation 8 in ref. 12). The fact that we find a relatively low  $g_{\text{i,COS}}$  compared with  $g_{\text{s,COS}}$  during the daytime implies that  $g_{\text{i,COS}}$  has a relatively large control on  $F_{\text{CO}_2}$ . Wehr et al. (23) estimated that the biochemical conductance (the CA activity) was of similar magnitude as  $g_{\text{s,COS}}$  during the daytime. The fact that we also find a relatively high importance of  $g_{\text{i,COS}}$  emphasizes the need to take into account  $g_{\text{i,COS}}$  on the total conductance of COS uptake (17). The day–night difference of  $g_{\text{s,COS}}$  is larger than that of  $g_{\text{i,COS}}$ , and therefore  $g_{\text{s,COS}}$  has a relatively larger effect on day–night differences of  $F_{\text{CO}_2}$  than  $g_{\text{i,COS}}$  has. This means that the diurnal change of  $F_{\text{CO}_2}$  is largely controlled by  $g_{\text{s,COS}}$ . Furthermore,  $g_{\text{i,COS}}$  has a relatively larger limiting role on  $F_{\text{CO}_2}$  during daytime than during nighttime (*SI Appendix, Fig. S4*). This variable role of  $g_{\text{i,COS}}$  over a day explains why the relation between  $F_{\text{CO}_2}$  and  $g_{\text{s,COS}}$  is different between different moments of the day, as depicted by different light levels in Fig. 2 E and F. If  $F_{\text{CO}_2}$  is used to determine  $g_{\text{s,COS}}$ ,

and the limiting role of  $g_{\text{i,COS}}$  on  $F_{\text{CO}_2}$  is ignored, this would lead to underestimation of daytime  $g_{\text{s,COS}}$ . When the  $F_{\text{CO}_2}$ – $g_{\text{s,COS}}$  relationship is assumed to be the same for daytime and nighttime (following the blue curve in Fig. 2 E and F),  $g_{\text{s,COS}}$  would be equal to 0.012 and 0.020  $\text{mol m}^{-2}\text{s}^{-1}$  for chambers 1 and 2, respectively, at  $F_{\text{CO}_2}$  of  $-3 \text{ pmol m}^{-2}\text{s}^{-1}$  (the average  $F_{\text{CO}_2}$  at high light levels). These values are, respectively, 46% and 48% smaller than what is actually observed (following the orange curve in Fig. 2 E and F). Therefore, ignoring the role of  $g_{\text{i,COS}}$  would lead to a substantial underestimation of  $g_{\text{s,COS}}$ .

### Seasonal Variation of LRU Influenced by Environmental Variables.

Fig. 3 shows the light-saturated LRU per month binned by VPD. The monthly median LRU decreases by 0.2 from April to July. No significant correlation between LRU and VPD can be detected before June, whereas a significant decrease of LRU with VPD is observed in June and July (indicated by the significance levels in Fig. 3). The fact that the LRU–VPD correlation follows the progression of the growing season is associated with the increase of daytime VPD. Early in the season  $F_{\text{CO}_2}$  and  $F_{\text{CO}_2}$  are not solely limited by stomatal conductance but rather by low temperatures, as is shown in *SI Appendix, Fig. S5*. The low temperatures suppress enzyme activities or mesophyll diffusion and therefore  $g_{\text{i,COS}}$  has a relatively larger limiting effect on  $F_{\text{CO}_2}$  than  $g_{\text{s,COS}}$  early in the season. In the course of the season the limitation of VPD on stomatal conductance becomes stronger, which manifests in the LRU–VPD relationship. This emphasizes that the LRU– $g_{\text{s,COS}}$  correlation (*SI Appendix, Fig. S3*) only applies when both  $F_{\text{CO}_2}$  and  $F_{\text{CO}_2}$  are controlled by stomatal conductance; i.e., at high temperatures and high light conditions.

### Light and Humidity-Dependent LRU Required for Accurate COS-Based GPP Estimates.

In Fig. 4 we compare COS-based GPP estimates ( $\text{GPP}_{\text{COS}}$ ) from COS ecosystem fluxes (determined from eddy-covariance measurements and subtracted estimates of the soil flux) with GPP from a traditional flux-partitioning method based on extrapolating nighttime respiration to the daytime (28) ( $\text{GPP}_{\text{NEE}}$ ).  $\text{GPP}_{\text{COS}}$  is determined using different parameterizations of LRU: (i) a fit of the measured LRU (averaged over chambers 1 and 2) against PAR, which captures the decrease of LRU toward simultaneously increasing VPD and PAR ( $\text{GPP}_{\text{COS-fit}}$ ; see *SI Appendix, Fig. S6* for the LRU–PAR relationship) and (ii) LRU fixed at 1.1 (the average LRU that we find at high light levels) and 1.6 [similar to what has been frequently used in other literature (7, 15, 29)], where the latter is shown in Fig. 4 as  $\text{GPP}_{\text{COS-const}}$ . The shading of the GPP estimates represents the uncertainty based on Monte Carlo sampling of all parameters contributing to the GPP calculations (*Methods*). The  $\text{GPP}_{\text{COS}}$  uncertainty is larger than that of  $\text{GPP}_{\text{NEE}}$ , partly because the relative uncertainty of COS mole fraction measurements ( $\sim 1.7\%$  of a typical ambient level of 450 ppt) is greater than that of  $\text{CO}_2$  mole fraction measurements ( $\sim 0.06\%$  of a typical value of 400 ppm) (30). Still, Fig. 4 shows that the accuracy of  $\text{GPP}_{\text{COS}}$  is sufficient to detect differences between  $\text{GPP}_{\text{COS}}$  and  $\text{GPP}_{\text{NEE}}$ . We also calculated  $\text{GPP}_{\text{COS}}$  with the measured hourly LRU to determine to what extent uncertainty in the LRU–PAR function adds uncertainty to  $\text{GPP}_{\text{COS-fit}}$ . The uncertainties did not decrease with measured LRU values compared with the LRU–PAR function, implying that the empirical function captures the variability of LRU over the measurement period well.

With the constant LRU, the earlier peak of  $F_{\text{CO}_2}$  leads to an earlier peak in  $\text{GPP}_{\text{COS-const}}$  compared with  $\text{GPP}_{\text{NEE}}$ . The peak of ecosystem  $F_{\text{CO}_2}$ , and thus that of  $\text{GPP}_{\text{COS-const}}$  is 2 h later than the peak of  $F_{\text{CO}_2}$  measured at the branch level at the top of the canopy. The reason for the delay between the  $F_{\text{CO}_2}$  peak from branches and ecosystem is that the diurnal pattern of the bulk canopy conductance is more symmetric, because light rather than  $g_{\text{s}}$  is limiting  $\text{CO}_2$  assimilation in the lower canopy, in contrast to the top of the canopy (31). When  $\text{GPP}_{\text{COS}}$  is calculated with the average LRU that we find at high light levels (1.1), we find  $\text{GPP}_{\text{COS}}$  ( $13.4 \pm 1.3 \text{ g C m}^{-2}\text{d}^{-1}$ ; daytime data only) to



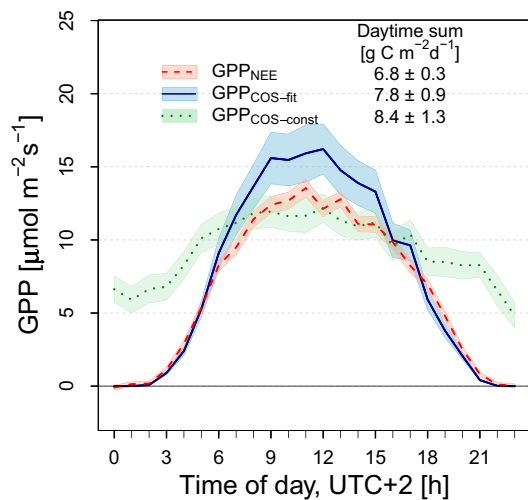


**Fig. 4.** GPP estimates based on COS and standard methods. Diurnal cycles of GPP between 18 May and 13 July 2017 based on NEE partitioning ( $GPP_{NEE}$ ; red) and observed COS ecosystem fluxes [using EC measurements with soil flux estimates subtracted (45)] following Eq. 1 ( $GPP_{COS}$ ). For  $GPP_{COS}$ , LRU is determined with two different representations: from a PAR-dependent fit (*SI Appendix*, Fig. S6) of LRU based on the continuous branch measurements, where the average of chambers 1 and 2 is taken ( $GPP_{COS-fit}$ ; blue); LRU fixed at 1.6 ( $GPP_{COS-const}$ ; green), which is similar to what has been frequently used in other literature (7, 15, 29). The averages (thick lines) and uncertainties (shaded areas) are based on 1,000 subsamples of Monte Carlo simulations that include uncertainties of all contributing components in the GPP calculation in each bin (*Methods*). We calculated the summed GPP from the average diurnal cycle for each representation (for daytime data only), which is shown in the top right corner.

with environmental variables and phenological stages must be incorporated to obtain accurate estimates of GPP from COS measurements. The LRU–PAR relationship found in this study can help to scale up LRU to ecosystem, regional, and global scales. Furthermore, the close relationship between  $F_{COS}$  and  $g_s$  that we observed can provide additional constraints to both the carbon and water cycles. With recent efforts to characterize sources and sinks of COS in ecosystems, accurate COS-based GPP estimates are now within reach and will allow testing and validation of other flux-partitioning methods.

## Methods

**Branch Measurements.** Measurements were performed at the Station for Measuring Ecosystem–Atmosphere Relations II (SMEAR II) in Hyttälä, Finland (61°51' N, 24°17' E, 181 m above sea level), which is dominated by Scots pine (*Pinus sylvestris* L.) (40). Four automated gas-exchange chambers were installed at the top of the canopy in two Scots pine trees between February 16 and July 17, 2017; details of those chamber measurements are provided in *SI Appendix*. PAR was measured by quantum sensors (Li-Cor LI-190) inside and outside the chambers. Temperature sensors (thermocouples and PT100) were placed inside the chambers. During measurements, the chambers were closed for 4 min and each chamber was measured once every hour. Air was pumped through a 4-mm (inner) diameter Synflex (Decabon) tube of 65-m length from the branch chambers to a quantum cascade laser spectrometer (QCLS) (Aerodyne Research Inc.) with a flow of 1–1.5 L min<sup>−1</sup> which was constantly recorded with Honeywell flowmeters (AWM5101VN). No active supply flow was provided, but ambient air could enter the chamber through small holes in the chamber housing (41). The sample tubing outside the instrumentation cabin was heated to prevent condensation on the tubing walls. The QCLS measured COS, CO<sub>2</sub>, CO, and H<sub>2</sub>O mole fractions (1 Hz) from the branch chambers along with half-hourly cylinder measurements for calibration. We corrected for the spectral water vapor interference of COS (30). The overall uncertainty including scale transfer, water vapor corrections, and measurement precision was determined to be 7.5 parts per trillion for COS and 0.23 parts per million for CO<sub>2</sub> (30). More information about the instrumentation and the calibration method can be found in Kooijmans

et al. (30) and the deployment of the instrument at the SMEAR II station in Kooijmans et al. (42).

Fluxes were calculated from the change of molar concentrations within the chamber during chamber closure through the following mass balance equation:

$$V \frac{dC}{dt} = FA + q(C_a - C), \quad [2]$$

where  $C$  is the molar concentration of each species inside the chamber (mol m<sup>−3</sup>),  $C_a$  the ambient molar concentration (mol m<sup>−3</sup>),  $V$  the chamber volume (m<sup>3</sup>),  $F$  the uptake or emission rate (mol m<sup>−2</sup> s<sup>−1</sup>),  $A$  the leaf area (m<sup>2</sup>), and  $q$  the flow rate (m<sup>3</sup> s<sup>−1</sup>). The measured mole fractions of the gas species (mol mol<sup>−1</sup>) are converted to molar concentrations using the ideal gas law with average temperature during chamber closure and pressure measurements at the site. The fluxes were calculated from least-square fit of the time series of molar concentrations inside the chamber and by solving Eq. 2.  $C_a$  was determined from open chamber measurements during a few minutes before chamber closure.

We measured fluxes in empty chambers (called “blank” measurements) to test and correct for gas exchange by the chamber and possibly by tubing materials. We measured blanks for all chambers in July and during a few days in March, May, and June. The fluxes were corrected for the blank emissions as is further described in *SI Appendix*.

In *SI Appendix* we also discuss the effect of leaf mitochondrial respiration on  $F_{CO_2}$  and LRU. Since we do not have the means to quantify diurnal changes of leaf mitochondrial respiration we approximate leaf-level LRU with the observed  $F_{CO_2}$ .

**Stomatal Conductance.** With transpiration measurements ( $F_{H_2O}$ ) available, we would ideally calculate stomatal conductance to water vapor ( $g_{s,H_2O}$ ) from  $F_{H_2O}$  normalized by VPD, where  $F_{H_2O}$  is simultaneously determined along with  $F_{CO_2}$  and  $F_{CO_2}$  from the branch chamber measurements. However, in chamber measurements, transpiration is underestimated at high relative humidity (RH) levels because the transpired water vapor can get adsorbed on the chamber walls. Measurements of  $F_{H_2O}$  therefore may not provide reliable  $g_{s,H_2O}$  estimates at high humidity levels. Therefore, we determined  $g_{s,H_2O}$  from the Ball–Berry model where the empirical slope ( $m$ ) and intercept ( $g_0$ ) parameters are determined from  $g_{s,H_2O}$ , which is determined with  $F_{H_2O}$  and VPD under low-humidity conditions. We use a threshold for RH (70%) to avoid the effect of condensation on the chamber walls. The Ball–Berry model describes  $g_{s,H_2O}$  as function of  $F_{CO_2}$ , RH and the atmospheric CO<sub>2</sub> mole fraction (43):

$$g_{s,H_2O} = m \cdot F_{CO_2} \cdot \frac{RH}{C_{a,CO_2}} + g_0. \quad [3]$$

The model parameters  $m$  and  $g_0$  are determined through linear regression with an  $R^2$  of 0.98 and 0.99 for chambers 1 and 2, respectively. With the regression being linear, we do not expect that using the Ball–Berry model rather than the measured  $g_{s,H_2O}$  leads to a bias in the results. As the Ball–Berry model does not allow for  $g_{s,H_2O}$  estimates in the dark when there is no photosynthesis, we determined the nighttime  $g_{s,H_2O}$  based on  $F_{H_2O}$  normalized by VPD (for RH < 70%). The leaf temperature used for VPD was calculated from a leaf energy balance model that incorporated heating by incoming shortwave radiation and cooling by transpiration and sensible heat transfer (44). The RH used for VPD calculations was determined from water vapor mole fractions in the open chamber a few minutes before chamber closure.

**GPP Estimates.** We determined GPP from NEE and extrapolated nighttime respiration following the traditional flux-partitioning method in Reichstein et al. (28). In addition to these NEE-based GPP estimates, we calculated GPP through Eq. 1 using different representations of LRU: with a PAR-dependent fit to the measured LRU (*SI Appendix*, Fig. S6) and with LRU fixed at 1.1 and 1.6. Vegetative COS fluxes were determined from eddy-covariance (EC) measurements in 2017 and soil COS fluxes that were characterized at the site in 2015 (45). The EC measurements of COS fluxes were made with a second QCLS of the same make at 10-Hz frequency together with a sonic anemometer (Solent Research HS1199; Gill Ltd.) at 23-m height. EC fluxes of COS were calculated from COS mixing ratios (corrected for water vapor in air) using the EddyUH software package developed at the University of Helsinki (46). Storage fluxes were estimated from mole fractions at 18 m assuming a constant height profile. More details about the flux and storage calculation procedure can be found in Kooijmans et al. (42). Data with low friction velocity (<0.3 m s<sup>−1</sup>) were filtered out. Soil COS fluxes were measured in 2015 at the Hyttälä site and showed no seasonal or diurnal cycle (45). An average

soil flux of  $-2.7 \text{ pmol m}^{-2}\text{s}^{-1}$  was subtracted from the ecosystem fluxes such that the remaining flux represents the vegetative COS exchange. The averages and uncertainties shown in Fig. 4 are based on 1,000 subsamples of Monte Carlo simulations that include uncertainties of all contributing components in the GPP calculation. That is, the SE of  $F_{\text{COS-EC}}$  and NEE; the COS soil flux uncertainty of  $1.1 \text{ pmol m}^{-2}\text{s}^{-1}$  (45); the SE of the fitting parameters of the LRU-PAR relation (using the median PAR in the calculation), or no uncertainty in LRU in the case of a constant LRU; the uncertainties of COS and  $\text{CO}_2$  mole fractions of 6.0 ppt and 0.13 ppm respectively (30), and the range of respiration calculations from figure 11 in ref. 47.

**Meteorological Data.** In addition to the temperature and PAR sensors installed at the branch chambers we use the data that are made available through the SmartSMEAR database that contains continuous data records from all SMEAR sites (available at <https://avaa.tdata.fi>).

**Statistical Tests.** The significance of correlations is tested with two-sided  $t$  tests of which the significance levels ( $P$ ) are reported. To reduce the effect

of outliers we test the linear correlation of data based on bin-averaged medians, where the bins are of equal size. The number of samples of the original data are reported for each  $t$  test. The number of bins are mentioned in figure legends.

**Code and Data Availability.** Data and code related to this paper are available in refs. 48–50.

**ACKNOWLEDGMENTS.** We thank the technical staff at the SMEAR II station in Hyttälä and M. de Vries, B. A. M. Kers, H. A. Been, and H. G. Jansen from the University of Groningen for their help during preparation and maintenance of the field campaign. This research was supported by the Startup Grant (awarded to H.C.) at the University of Groningen, the National Oceanic and Atmospheric Administration Climate Program Office Grant (NA13OAR4310082), the European Union's Horizon 2020 research and innovation program (Grant 654182), the Vilho, Yrjö, and Kalle Väisälä Foundation, Integrated Carbon Observation System-Finland (Grant 281255), Academy of Finland Center of Excellence program (307331), and the NSF CAREER Award 1455381 (to U.S.).

- Protoschill-Krebs G, Wilhelm C, Kesselmeier J (1992) Enzymatic pathways for the consumption of carbonyl sulphide (COS) by higher plants. *Bot Acta* 105:206–212.
- Protoschill-Krebs G, Wilhelm C, Kesselmeier J (1996) Consumption of carbonyl sulphide (COS) by higher plant carbonic anhydrase (CA). *Atmos Environ* 30:3151–3156.
- Notni J, Schenk S, Protoschill-Krebs G, Kesselmeier J, Anders E (2007) The missing link in COS metabolism: A model study on the reactivation of carbonic anhydrase from its hydrosulfide analogue. *Chembiochem* 8:530–536.
- Montzka SA, et al. (2007) On the global distribution, seasonality, and budget of atmospheric carbonyl sulfide (COS) and some similarities to  $\text{CO}_2$ . *J Geophys Res Atmos* 112:D09302.
- Campbell JE, et al. (2008) Photosynthetic control of atmospheric carbonyl sulfide during the growing season. *Science* 322:1085–1088.
- Berry J, et al. (2013) A coupled model of the global cycles of carbonyl sulfide and  $\text{CO}_2$ : A possible new window on the carbon cycle. *J Geophys Res Biogeosci* 118:842–852.
- Asaf D, et al. (2013) Ecosystem photosynthesis inferred from measurements of carbonyl sulphide flux. *Nat Geosci* 6:186–190.
- Sandoval-Soto L, et al. (2005) Global uptake of carbonyl sulfide (COS) by terrestrial vegetation: Estimates corrected by deposition velocities normalized to the uptake of carbon dioxide ( $\text{CO}_2$ ). *Biogeosciences* 2:125–132.
- Kesselmeier J, Merk L (1993) Exchange of carbonyl sulfide (COS) between agricultural plants and the atmosphere: Studies on the deposition of COS to peas, corn and rapeseed. *Biogeochemistry* 23:47–59.
- Kesselmeier J, et al. (1993) Reduced sulfur compound exchange between the atmosphere and tropical tree species in Southern Cameroon. *Biogeochemistry* 23:23–45.
- Kuhn U, et al. (1999) Carbonyl sulfide exchange on an ecosystem scale: Soil represents a dominant sink for atmospheric COS. *Atmos Environ* 33:995–1008.
- Seibt U, Kesselmeier J, Sandoval-Soto L, Kuhn U, Berry JA (2010) A kinetic analysis of leaf uptake of COS and its relation to transpiration, photosynthesis and carbon isotope fractionation. *Biogeosciences* 7:333–341.
- Stimler K, Montzka SA, Berry JA, Rudich Y, Yakir D (2010) Relationships between carbonyl sulfide (COS) and  $\text{CO}_2$  during leaf gas exchange. *New Phytol* 186:869–878.
- Stimler K, Berry JA, Montzka SA, Yakir D (2011) Association between carbonyl sulfide uptake and  $(\delta^{18}\text{O})$  during gas exchange in C(3) and C(4) leaves. *Plant Physiol* 157:509–517.
- Stimler K, Berry JA, Yakir D (2012) Effects of carbonyl sulfide and carbonic anhydrase on stomatal conductance. *Plant Physiol* 158:524–530.
- Berkelhammer M, et al. (2014) Constraining surface carbon fluxes using in situ measurements of carbonyl sulfide and carbon dioxide. *Global Biogeochem Cycles* 28:161–179.
- Sun W, Maseyk K, Lett C, Seibt U (2018) Stomatal control of leaf fluxes of carbonyl sulfide and  $\text{CO}_2$  in a Typha freshwater marsh. *Biogeosciences* 15:3277–3291.
- Whelan ME, et al. (2018) Reviews and syntheses: Carbonyl sulfide as a multi-scale tracer for carbon and water cycles. *Biogeosciences* 15:3625–3657.
- Maseyk K, et al. (2014) Sources and sinks of carbonyl sulfide in an agricultural field in the Southern Great Plains. *Proc Natl Acad Sci USA* 111:9064–9069.
- Commane R, et al. (2015) Seasonal fluxes of carbonyl sulfide in a midlatitude forest. *Proc Natl Acad Sci USA* 112:14162–14167.
- Gries C, Nash TH, Kesselmeier J (1994) Exchange of reduced sulfur gases between lichens and the atmosphere. *Biogeochemistry* 26:25–39.
- Protoschill-Krebs G, Wilhelm C, Kesselmeier J (1995) Consumption of carbonyl sulphide by chlamydomonas reinhardtii with different activities of carbonic anhydrase (CA) induced by different  $\text{CO}_2$  growing regimes. *Bot Acta* 108:445–448.
- Wehr R, et al. (2017) Dynamics of canopy stomatal conductance, transpiration, and evaporation in a temperate deciduous forest, validated by carbonyl sulfide uptake. *Biogeosciences* 14:389–401.
- Geng C, Mu Y (2006) Carbonyl sulfide and dimethyl sulfide exchange between trees and the atmosphere. *Atmos Environ* 40:1373–1383.
- Farquhar GD, von Caemmerer S, Berry JA (1980) A biochemical model of photosynthetic  $\text{CO}_2$  assimilation in leaves of C 3 species. *Planta* 149:78–90.
- Cowan IR, Farquhar GD (1977) Stomatal function in relation to leaf metabolism and environment. *Symp Soc Exp Biol* 31:471–505.
- Farquhar GD (1982) Stomatal conductance and photosynthesis. *Annu Rev Plant Physiol* 33:317–345.
- Reichstein M, et al. (2005) On the separation of net ecosystem exchange into assimilation and ecosystem respiration: Review and improved algorithm. *Glob Change Biol* 11:1424–1439.
- Hilton T, et al. (2017) Peak growing season gross uptake of carbon in North America is largest in the Midwest USA. *Nat Clim Chang* 7:450–454.
- Kooijmans LMJ, et al. (2016) Continuous and high-precision atmospheric concentration measurements of COS,  $\text{CO}_2$ , CO and  $\text{H}_2\text{O}$  using a quantum cascade laser spectrometer (QCLS). *Atmos Meas Tech* 9:5293–5314.
- Launiainen S, Katul GG, Kolari P, Vesala T, Hari P (2011) Empirical and optimal stomatal controls on leaf and ecosystem level  $\text{CO}_2$  and  $\text{H}_2\text{O}$  exchange rates. *Agric For Meteorol* 151:1672–1689.
- Wehr R, et al. (2016) Seasonality of temperate forest photosynthesis and daytime respiration. *Nature* 534:680–683.
- Wilkman E, et al. (2018) Temperature response of respiration across the heterogeneous landscape of the Alaskan Arctic tundra. *J Geophys Res Biogeosci* 123:2287–2302.
- Huang K, et al. (2014) Impacts of diffuse radiation on light use efficiency across terrestrial ecosystems based on eddy covariance observation in China. *PLoS One* 9:e110988.
- Thornton PE, Lamarque J-F, Rosenbloom NA, Mahowald NM (2007) Influence of carbon-nitrogen cycle coupling on land model response to  $\text{CO}_2$  fertilization and climate variability. *Global Biogeochem Cycles* 21:1–15.
- Krinner G, et al. (2005) A dynamic global vegetation model for studies of the coupled atmosphere-biosphere system. *Global Biogeochem Cycles* 19:GB1015.
- Sitch S, et al. (2004) Evaluation of ecosystem dynamics plant geography and terrestrial carbon cycling in the LPJ dynamic global vegetation model. *Glob Change Biol* 9:161–185.
- Launois T, Peylin P, Belviso S, Poulter B (2015) A new model of the global biogeochemical cycle of carbonyl sulfide—Part 2: Use of carbonyl sulfide to constrain gross primary productivity in current vegetation models. *Atmos Chem Phys* 15:9285–9312.
- Yang F, Qubaja R, Tatarinov F, Rotenberg E, Yakir D (2018) Assessing canopy performance using carbonyl sulfide measurements. *Glob Change Biol* 24:3486–3498.
- Bäck J, et al. (2012) Chemodiversity of a Scots pine stand and implications for terpene air concentrations. *Biogeosciences* 9:689–702.
- Aalto J, et al. (2014) New foliage growth is a significant, unaccounted source for volatiles in boreal evergreen forests. *Biogeosciences* 11:1331–1344.
- Kooijmans LMJ, et al. (2017) Canopy uptake dominates nighttime carbonyl sulphide fluxes in a boreal forest. *Atmos Chem Phys* 17:11453–11465.
- Ball JT, Woodrow IE, Berry JA (1987) A model predicting stomatal conductance and its contribution to the control of photosynthesis under different environmental conditions. *Progress in Photosynthesis Research*, ed Biggens J (Springer, Dordrecht, The Netherlands), Vol 4, pp 221–224.
- Nobel PS (2009) *Physicochemical and Environmental Plant Physiology* (Academic, Oxford).
- Sun W, et al. (2018) Soil fluxes of carbonyl sulfide (COS), carbon monoxide, and carbon dioxide in a boreal forest in Southern Finland. *Atmos Chem Phys* 18:1363–1378.
- Mammarella I, Peltola O, Nordbo A, Järvi L, Rannik Ü (2016) Quantifying the uncertainty of eddy covariance fluxes due to the use of different software packages and combinations of processing steps in two contrasting ecosystems. *Atmos Meas Tech* 9:4915–4933.
- Kolari P, et al. (2009)  $\text{CO}_2$  exchange and component  $\text{CO}_2$  fluxes of a boreal Scots pine forest. *Boreal Environ Res* 14:761–783.
- Kooijmans LMJ (2018) Code for “Influences of light and humidity on carbonyl sulfide-based estimates of photosynthesis.” Zenodo. Available at <https://zenodo.org/record/1211499#.XEC-zFVKgdV>. Deposited April 3, 2018.
- Kooijmans LMJ, et al. (2018) Dataset for “Influences of light and humidity on carbonyl sulfide-based estimates of photosynthesis.” Zenodo. Available at <https://zenodo.org/record/1211481#.XEC-NVVKhQJ>. Deposited April 3, 2018.
- Sun W (2018) Code for calculation of chamber fluxes: “PyChamberFlux.” Zenodo. Available at <https://zenodo.org/record/1197330#.XEC-i1VKgdV>. Deposited March 13, 2018.